NANO LETTERS

2004
Vol. 4, No. 11
2151−2155

Magnetite (Fe_3O_4) Core–Shell Nanowires: Synthesis and Magnetoresistance

Daihua Zhang,[†,§] Zuqin Liu,[†,§] Song Han,[†] Chao Li,[†] Bo Lei,[†] Michael P. Stewart,[‡,||] James M. Tour,[‡] and Chongwu Zhou*[,†]

Department of E.E.-Electrophysics, University of Southern California, Los Angeles, California 90089, and Department of Chemistry and Center for Nanoscale Science and Technology, Rice University, Houston, Texas 77005

Received August 1, 2004; Revised Manuscript Received October 1, 2004

ABSTRACT

High quality MgO/Fe_3O_4 core−shell nanowires have been successfully synthesized by depositing an epitaxial shell of Fe_3O_4 onto single crystal MgO nanowires. The material composition and stoichoimetric ratio have been carefully examined and confirmed with a variety of characterization techniques. These novel structures have rendered unique opportunities to investigate the transport behavior and spintronic property of Fe_3O_4 in its one-dimensional form. Room-temperature magnetoresistance of ∼1.2% was observed in the as-synthesized nanowires under a magnetic field of $B = 1.8$ T, which has been attributed to the tunneling of spin-polarized electrons across the anti-phase boundaries.

As has been theoretically predicted on the basis of electron band structure calculations, magnetite (Fe_3O_4) represents a family of materials that fall into the category of half metals, where the electronic density of states is 100% spin polarized at the Fermi level.[1−3] Because of the high spin polarization, combined with its favorable Curie temperature ($T_C = 850$ K), Fe_3O_4 has been attracting quite extensive research efforts in the past decades.[4,5] Despite its promising applications in spintronics/electronics, e.g., spin injection electrodes in tunneling magnetoresistance (TMR) devices,[6−8] a number of intriguing properties arising from the spin-polarized transport, in particular, the magnetoresistance (MR) observed in certain Fe_3O_4 systems, have not been well understood thus far. Previous electron transport and MR studies have been mainly focused on different forms of Fe_3O_4 including epitaxial[9−13] and polycrystalline thin films,[13−17] nanocluster assemblies,[18−21] and compacted powders,[14] where the MR was ascribed to the tunneling of spin-polarized electrons across the antiferromagnetically coupled antiphase/grain boundaries or interparticle contacts. However, none of the above device structures, which contain too many randomly distributed tunneling barriers and complex transport channels, turns out to be an ideal model for the MR investigations. The proposed mechanism thus remains at a qualitative or, at most, semiquantitative level due to the lack of properly structured devices.

Ideally, quasi one-dimensional (1D) structures of Fe_3O_4, where the magnetic domains, single-crystalline grains, or nanocrystals are aligned in series, are highly desired for the MR studies. In a 1D wire, the electron transport path, and even the number/positions of tunneling boundaries, could be determined, hence circumventing the uncertainty and complexity in the two-dimensional (2D) thin films. Nevertheless, despite few approaches reported recently,[22−24] a mature and controllable synthesis technique for the 1D Fe_3O_4 nanostructures has not been available, not to mention any study on their transport properties. Very recently, a great opportunity has been opened up by a newly developed synthesis technique in our group to produce a collection of transition metal oxide "core−shell" nanowires.[25] Instead of a 2D single crystal MgO template that is typically used for obtaining an epitaxial Fe_3O_4 thin film, we have successfully produced MgO/Fe_3O_4 core−shell nanowires by epitaxially depositing an Fe_3O_4 shell layer onto MgO nanowires serving as the supporting cores. With the as synthesized core−shell nanowires, we are now capable of investigating the transport behavior of Fe_3O_4 in its quasi 1D systems. This novel synthesis technique not only provided well-defined 1D transport channels but readily introduced antiphase boundaries (APBs) in the Fe_3O_4 shell layer, which have been proven to be the cause for the MR in epitaxial Fe_3O_4 thin films. More importantly, understanding and optimizing these nanoscaled MR devices are also meaningful tasks for their

* Corresponding author. E-mail: chongwuz@usc.edu.
† University of Southern California.
‡ Rice University.
|| Now at Intel Corporation, Santa Clara, CA.
§ These authors contributed equally.

10.1021/nl048758u CCC: $27.50
Published on Web 10/22/2004

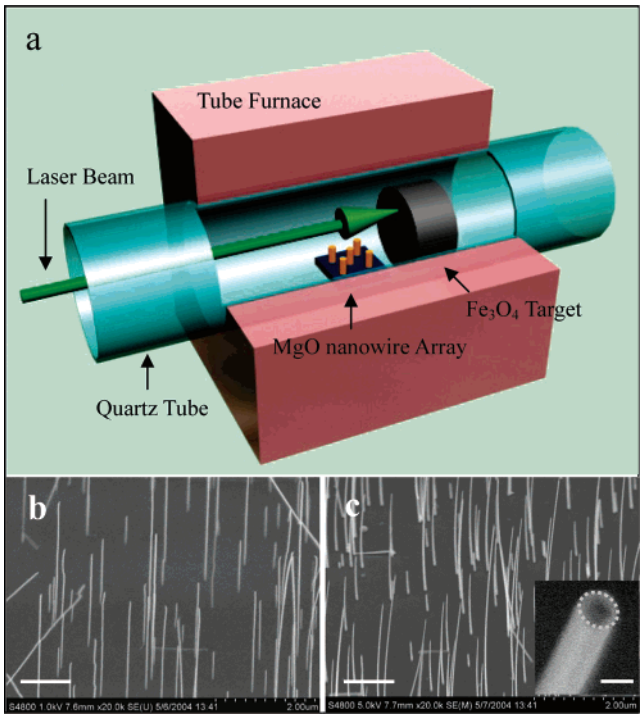

Figure 1. (a) Schematic drawing of the PLD system used for the Fe_3O_4 deposition, (b) SEM image of the vertical MgO nanowires, and (c) the MgO/Fe_3O_4 core−shell nanowires. (Inset) Top view SEM image showing the circular cross section of the core−shell nanowire. Scale bars: 1 μm, 1 μm, and 20 nm for (b), (c) and the inset, respectively.

direct applications in nanoelectronics/spintronics, e.g., Fe_3O_4 nanowire-based magnetic field read heads with ultrahigh spatial resolutions.

We present here our recent studies on these Fe_3O_4 core−shell nanowires. Following the synthesis, various characterization techniques have been utilized to confirm the magnetite material composition and stoichiometry. In addition, four-point probe devices based on single magnetite nanowires have been synthesized and systematically studied for the first time, and room-temperature magnetoresistance has been demonstrated in such quasi 1D nanowires, with a ratio of ~1.2% at $B = 1.8$ T.

Vertically aligned MgO nanowire arrays, which work as the inner cores for the core−shell structure, were grown on single-crystal MgO (100) substrates following the vapor−liquid−solid mechanism. The experimental setup and detailed growth conditions have been described in our previous report.[25] A typical scanning electron microscope (SEM) image of the as-prepared samples is shown in Figure 1b, where the grown MgO nanowires were well separated and vertically aligned against the substrate. In addition to their uniform diameters and controllable lengths, a significant advantage of using these vertical MgO nanowires as the core template is that they do not shadow each other during the subsequent shell layer deposition, therefore ensuring a high-quality conformal coating of the core−shell nanowires.

The Fe_3O_4 shell layer deposition was performed in a pulsed laser deposition (PLD) system consisting of a tube furnace and a Nd:YAG laser (Figure 1a). The source target was compressed with Fe_3O_4 powders (Alfa Aesar, 99.99%), followed by post-annealing at 1000 °C in vacuum for 2 h. A frequency-doubled laser beam (532 nm) was used for ablation, with a repetition rate of 10 Hz and power density of 2−3 mW/cm^2 on the target. The vertical MgO nanowire array samples were positioned at 0.5 cm in front of the target under an ambient temperature of 350 °C to collect the product. The horizontal quartz tube was maintained at 7.5×10^{-2} Torr in a flow of Ar at 5 sccm opposite to the laser beam direction. We have estimated the deposition rate as ~2−3 Å/min. A growth time of 40 min has been typically used for obtaining a ~10 nm thick shell layer. After the deposition, we inspected the MgO nanowire sample again using SEM, with the image shown in Figure 1c. Most of the core−shell nanowires, as can be seen in the image, remained perpendicular to the MgO (100) substrate, with little change in their morphologies. The inset shows a high-magnification top view SEM image, demonstrating the circular cross section of the core−shell nanowires.

Building upon the knowledge of the PLD technique, the deposited shell layer was expected to possess the same chemical composition and stoichiometric ratio as in the Fe_3O_4 target. To confirm this, a variety of characterization techniques, including XRD, X-ray photoelectron spectroscopy (XPS), transmission electron microscopy (TEM), and energy-dispersive X-ray spectroscopy (EDS), have been used in the material analysis. Figure 2a plots the XRD data taken with the as-obtained samples, in which a strong and a much weaker peak were detected at $2\theta \approx 43.0°$ and 21.5°, corresponding to the MgO (200) and (400) planes. In the inset, we redrew the data in a zoom-in region from $2\theta =$ 41.5 ° to 44.5 ° (upper curve), for comparison with the lower curve recorded with a vertical MgO nanowire sample prior to Fe_3O_4 coating. We found that, in addition to the MgO (200) peak at $2\theta = 42.9$ °, another peak at $2\theta = 43.2$ ° was also detected, which has been indexed as Fe_3O_4 (400) plane via detailed analysis. The very small shift between the MgO (200) and Fe_3O_4 (400) peaks can be well interpreted as resulting from the nearly perfect lattice match between the two materials (0.3%), as both MgO and Fe_3O_4 take cubic crystal lattice with $a = 4.212$ Å for MgO and 8.397 Å for Fe_3O_4.[26] In addition, the lack of diffraction peaks from other crystal planes further revealed the single-crystal nature of the epitaxial Fe_3O_4 layer deposited on both the MgO (100) substrate and the MgO core nanowires.

As an additional test to verify the presence of magnetite rather than maghemite (γ-Fe_2O_3), which has an almost identical XRD diffraction pattern, XPS was used to examine the Fe:O stoichiometry of the samples. The experiment was performed using non-monochromatic Al Kα radiation ($h\nu$ = 1486.6 eV) with the detector at 60° takeoff angle, probing a spot size of approximately 0.5 mm diameter. Figures 2b and 2c show the XPS signals of the Fe 2p and O 1s regions, together with their spectral deconvolution curves. Two peaks of Fe $2p_{1/2}$ at 710.6 eV and Fe $2p_{3/2}$ at 723.9 eV were observed, with the full width at half-maximum (FWHM) being 2.9 and 3.1 eV, respectively. The absence of the satellite peak situated at ~719 eV, which is a major characteristic of

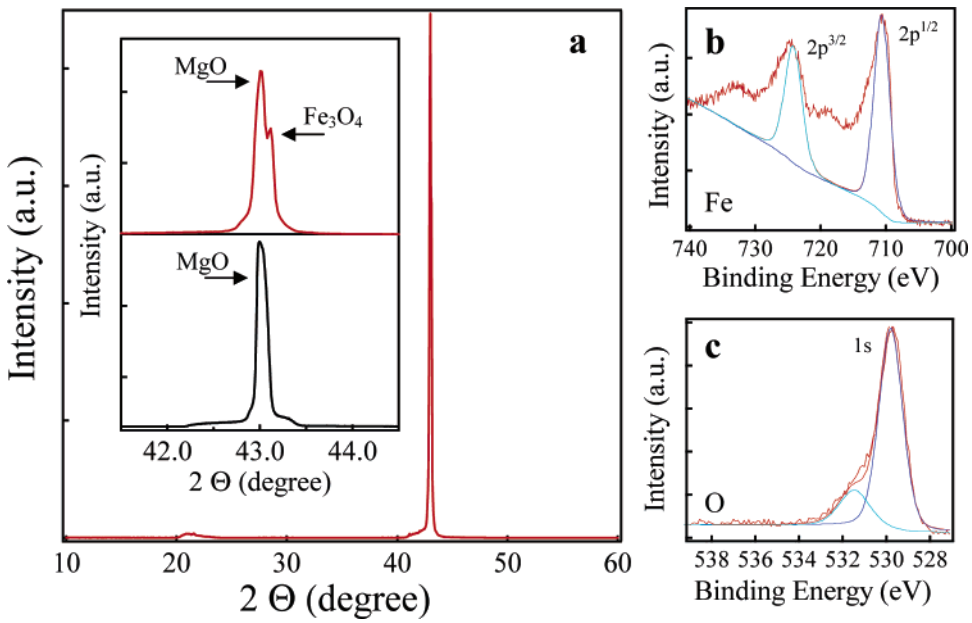

Figure 2. (a) XRD data of the as-obtained sample: MgO nanowires grown on MgO (100) substrate, with an epitaxial coating of Fe_3O_4. (Inset) Zoom-in view of the primary peak at $2\theta = 42° \sim 44°$, where a double-peak feature was clearly resolved (upper curve), in contrast to a single peak obtained with a bare MgO nanowire sample (lower curve). (b) XPS spectra: the lack of the $\pi \rightarrow \pi^*$ "shake-up" satellite peak confirms the material stoichiometry. The two peaks at 723.88 and 710.62 eV correspond to Fe $2p^{1/2}$ and $2p^{2/3}$, respectively. (c) XPS signal from oxygen.

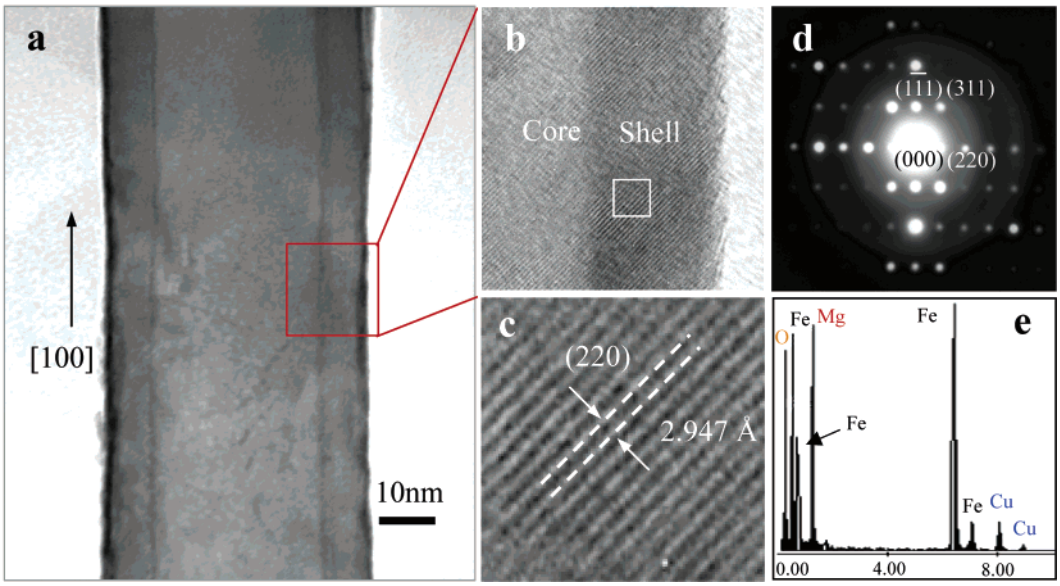

Figure 3. (a) TEM image of the core−shell nanowire showing the uniform Fe_3O_4 coating on the MgO core. The boxed region has been enlarged in (b) to inspect the core−shell interface. (c) The boxed area in (b) was further enlarged to examine the lattice spacing in the shell region. (d) SAED pattern of the core−shell nanowire. (e) EDX data recorded with the nanowire, where signals from Mg, Fe, and O were detected.

Fe^{3+} in γ-Fe_2O_3, clearly excluded the formation of γ-Fe_2O_3 in the epitaxial layer. The O core level spectrum in Figure 2c consisted of a mean peak originating from the oxygen in Fe_3O_4 (at 529.7 eV) and a shoulder centered at 531.3 eV, which has been ascribed to surface traps.[27] The Fe/O ratio of the epitaxial layer was estimated as 0.74 with curve resolution analysis, which matches well with the stoichiometric ratio of Fe_3O_4 (0.75). We note that in both the XPS and the XRD measurements, the signals came from the MgO/Fe_3O_4 core−shell nanowires and the epitaxial film on the substrates as well. The above characterization thus verifies the crystallinity and stoichiometry of both structures.

The morphology of the nanowires has been further investigated with TEM. Figure 3a shows a typical TEM image of the core−shell nanowire, indicating the uniform Fe_3O_4 coating on the MgO core. The diameter of the MgO core is ~25 nm and the thickness of coated shell is ~7 nm. By looking at the interface of the core and shell in the high resolution transmission electron microscopy (HRTEM) image (Figure 3b), we can find that the interface between the MgO

core and epitaxial magnetite shell appears relatively sharp. The lattice fringes are continuous from the core to the shell, confirming a perfect single-crystal epitaxial growth of the Fe_3O_4 layer. By analyzing the lattice fringes of the shell (shown in Figure 3c), the lattice spacing between two planes is ~2.947 Å, corresponding to the distance of two (220) planes of Fe_3O_4. The angle between the interface of core−shell and lattice fringe of (220) plane is determined to be 45°. This indicates that the axial growth direction core is along [100], consistent with our previous studies on MgO growth.[23] Figure 4d shows the $[1\bar{1}\bar{2}]$ zone axis electron diffracton pattern of the core−shell nanowires, further confirming the single-crystal nature. The corresponding nearest three spots in the figure can be indexed to (220), $(1\bar{1}1)$, and (311) planes of Fe_3O_4. EDX data (Figure 3e) have also been recorded with the nanowire, where signals from Mg, Fe, and O were detected.

These high quality MgO/Fe_3O_4 core−shell nanowires have rendered a unique opportunity to investigate the electron transport through Fe_3O_4 in a quasi 1D form. The transport studies have been carried out by measuring the four-probe resistance and MR of the core−shell nanowire devices, which were fabricated via the following techniques. We first sonicated the nanowires off the MgO substrate into 1-2-propanol, followed by dispersing the suspension onto a Si/SiO_2 substrate. E-beam lithography and thermoevaporation were then used to pattern and deposit four Ti/Au electrodes to contact the nanowires. The SEM image shown in Figure 4a is a perspective view of a typical device consisting of a 5 μm-long nanowire and four electrodes uniformly distributed on it. TEM studies performed with nanowires left in the suspension revealed the MgO diameter and the Fe_3O_4 shell thickness being ~20 nm and ~8 nm, respectively. Linear $I-V$ curves were obtained in four-probe measurements under a wide range of temperatures (Figure 4b), and the device resistance was derived as 0.8 MΩ at 290 K. Using a channel length of ~1 μm (between the middle two electrodes) and a cross section of $\sim 7 \times 10^{-12}$ cm^2 estimated from the shell geometry, we have deduced the resistivity of Fe_3O_4 in this quasi 1D form as $\sim 6 \times 10^{-2}$ Ω cm, which is in good agreement with the value for epitaxial thin films[8,10,11] but one order of magnitude higher than the bulk resistivity of 5×10^{-3} Ω cm.[28] This large discrepancy has been attributed to the presence of highly resistive APBs in the epitaxial layer, which are formed as growth defects due to the difference in the lattice constant between Fe_3O_4 and the underlying MgO substrate. Based upon Eerenstein's experimental results,[8] we have also estimated the thickness of the APBs to be ~2 nm and the size of each structural domain ~10 nm, for a ~8 nm thick epitaxial layer in our case. For simplicity, we can model the quasi 1D magnetite nanowire as a serial connection of domains (~10 nm wide) separated by APBs (~2 nm wide), as shown in the inset of Figure 4b. The conductivity of the APBs can therefore be calculated to be $\sigma_{APB} = 3$ $(\Omega cm)^{-1}$, matched very well with the estimation in ref 8, where $\sigma_{APB} = 2.0-2.3$ $(\Omega cm)^{-1}$ was obtained for 2 D Fe_3O_4 films. We note that detailed distribution of the APBs in these novel 1D magnetite nanowires awaits further experimental

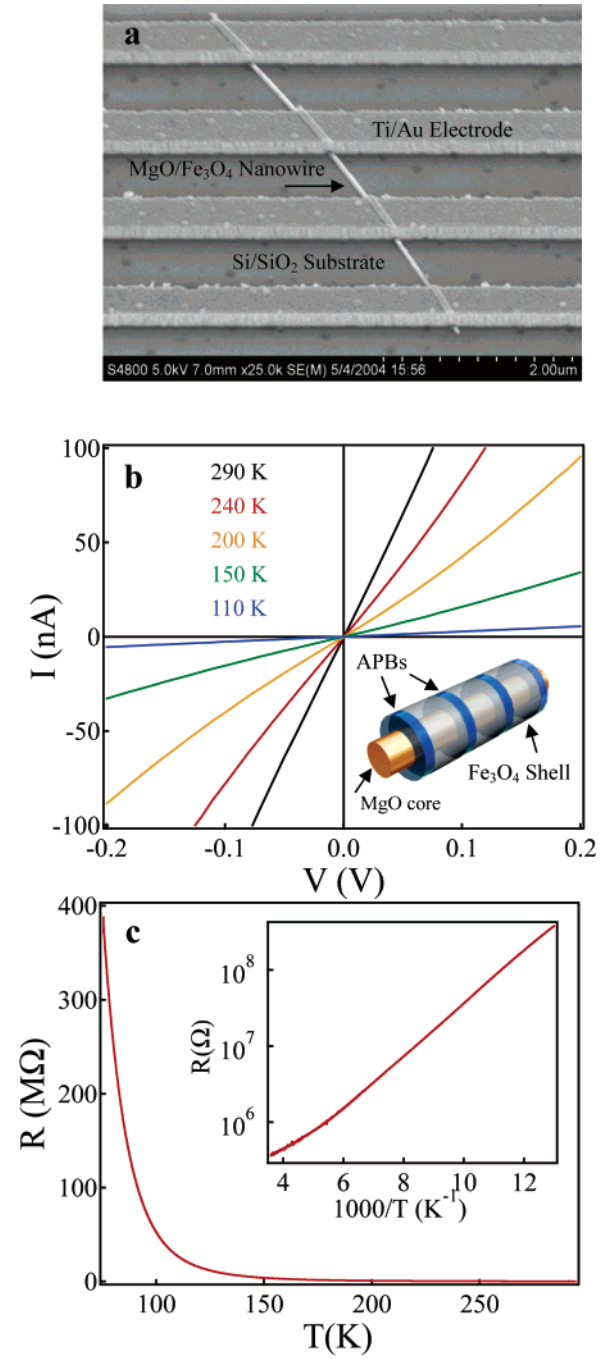

Figure 4. (a) SEM image shows a perspective view of the nanowire device, with four Ti/Au electrodes evenly distributed on the core−shell nanowire. (b) The four-probe $I-V$ curves taken at five different temperatures at $T = 290$, 240, 200, 150, and 110 K. (Inset) Proposed domain structure along the core−shell nanowire. (c) Resistance (R) vs temperature (T) measured with the as-fabricated four-electrode nanowire device. (Inset) R plotted as a function of $1/T$ in log scale.

and theoretical studies. In Figure 4c, the four-probe resistance was recorded as a function of temperature. The Arrhenius plot (ln R vs $1/T$ in the inset) shows a rather linear relation, suggesting a thermally activated hopping transport mechanism along the nanowire. An activation energy of $E_a \sim 0.1$ eV was estimated by fitting the curve using $R \sim \exp(-E_a/k_BT)$, where k_B is the Boltzmann constant. Also noteworthy is the absence of Verway transition in these core−shell nanowires, which has also been observed in very thin

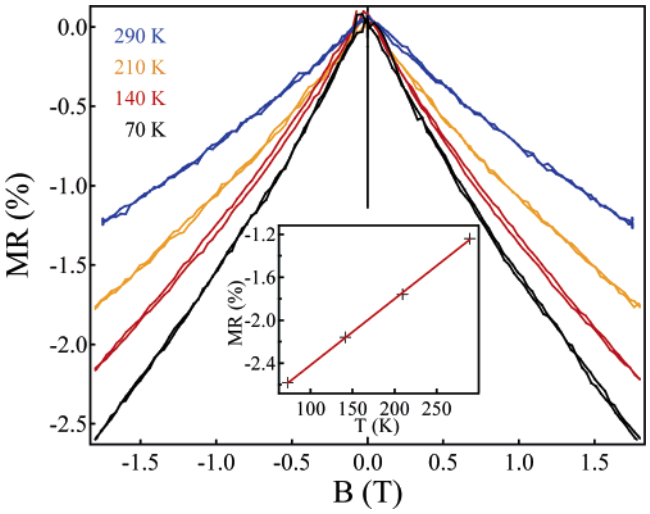

Figure 5. Magnetoresistance recorded at $T = 290$ K (blue), 210 K (yellow), 140 K (red), and 70 K (black), while a perpendicular magnetic field was double-swept between $B = \pm 1.8$ T. The magnetoresistance ratio at $B = 1.8$ T was also plotted as a function of temperature in the inset, which can be basically fitted into a straight line.

epitaxial Fe_3O_4 films (<30 nm).[8,9,11] It was suggested that in a system with high-density APBs and very small structural domains, the long-range order would be disturbed, thus preventing the occurrence of the phase transition at the Verwey temperature (T_v).

Finally, we performed MR measurements with the core−shell nanowire, with the data shown in Figure 5. The nanowire resistance was recorded at four different temperatures, while a perpendicular magnetic field was double-swept between $B = \pm 1.8$ T. MR of ~1.25% was achieved at $T = 290$ K and $B = 1.8$ T (corresponding to $H = 18$ kOe), and no saturation trend was observed within the scanned region. The obtained MR agrees with most previous studies on 2D Fe_3O_4 systems[7,10−13,15,17] As has been pointed out, the MR, either in 2D epitaxial films or the 1D form in our case, is believed to arise from the spin-polarized transport across the APBs, where the magnetic moments of B-site cations were antiferromagnetically coupled via a 180° superexchange interaction. A reduction in the resistivity is expected when the opposite moments at the APBs are slightly aligned by an applied magnetic field. In addition, the very strong antiferromagnetic (AF) coupling at the APBs induces very large saturation fields, which explains the absence of saturation in our measurements. The magnetoresistance ratio at $B = 1.8$ T was plotted vs T in the inset, where the MR monotonically increased with the decreasing temperature. This is understandable, as decreasing the temperature improves the alignment in the magnetic domains and also increases the degree of spin polarization near the Fermi level, and then contributes to an increase in the MR.

In summary, we have successfully synthesized MgO/Fe_3O_4 core−shell nanowires via the PLD technique. The material composition and stoichiometry have been examined and confirmed with various characterization techniques. For the first time, the transport behavior and MR property of this one-dimensionally structured Fe_3O_4 was investigated. Room-temperature MR of ~1.2% was observed in the nanowire at $B = 1.8$ T, which has been attributed to the tunneling of spin-polarized electrons across the APBs.

Acknowledgment. We thank Dr. Weigang Lu for his help on the TEM analysis. Prof. Keol and Mr. Thomas I. Valdez have offered valuable discussion regarding the XPS measurements. We gratefully acknowledge support from a NSF CAREER Award, a NSF-CENS grant, and a SRC MARCO/DARPA grant. Z.L. thanks the "WISE" postdoctoral fellowship of University of Southern California. J.M.T. thanks DARPA/ONR for support.

References

(1) de Groot, R. A.; Mueller, F. M.; van Engen, P. G.; Buschow, K. H. J. *Phys. Rev. Lett.* **1983**, *50*, 2024.
(2) Zhang, Z.; Satpathy, S. *Phys. Rev. B.* **1991**, *44*, 13319.
(3) Yanase, A.; Siratori, K. *J. Phys. Soc. Jpn.* **1984**, *53*, 312.
(4) Walz, F. *J. Phys.: Condens. Matter* **2002**, *14*, R285.
(5) Lu, Y.; Yin, Y. D.; Mayers, B. T.; Xia, Y. N. *Nano. Lett.* **2002**, *2*, 183.
(6) Batlle, X.; Cuadra, P. J.; Zhang, Z. Z.; Cardoso, S.; Freitas, P. P. *J. Magn. Magn. Mater.* **2003**, *261*, L305.
(7) Zhang, Z. Z.; Cardoso, S.; Freitas, P. P.; Batlle, X.; Wei, P.; Barradas, N.; Soares, J. C. *J. Appl. Phys.* **2001**, *89*, 6665.
(8) Kim, W.; Kawaguchi, K.; Koshizaki, N.; Sohma, M.; Mastsumoto, T. *J. Appl. Phys.* **2003**, *93*, 8032.
(9) Eerenstein, W.; Palstra, T. T. M.; Saxena, S. S.; Hibma, T. *Phys. Rev. Lett.* **2002**, *88*, 247204.
(10) Eerenstein, W.; Palstra, T. T. M.; Hibma, T.; Celitto, S. *Phys. Rev. B.* **2002**, *66*, 221101.
(11) Sena, S. P.; Lindley, R. A.; Blythe, H. J.; Sauer, Ch.; Al-Kafarji, M.; Gehring, G. A. *J. Magn. Magn. Mater.* **1997**, *176*, 111.
(12) Gong, G. Q.; Gupta, A.; Xiao, G.; Qian, W.; Dravid, V. P. *Phys. Rev. B* **1997**, *56*, 5096.
(13) Li, X. W.; Gupta, A.; Xiao, G.; Gong, G. Q. *J. Appl. Phys.* **1998**, *83*, 7049.
(14) Coey, J. M. D.; Berkowitz, A. E.; Balcells, L. I.; Putris, F. F.; Parker, F. T. *Appl. Phys. Lett.* **1998**, *72*, 734.
(15) Liu, H.; Jiang, E. Y.; Bai, H. L.; Zheng, R. K.; Zhang, X. X. *J. Phys. D: Appl. Phys.* **2003**, *36*, 2950.
(16) Hong, J. P.; Lee, S. B.; Jung, Y. W.; Lee, J. H.; Yoon, K. S.; Kim, K. W.; Kim, C. O.; Lee, C. H. *Appl. Phys. Lett.* **2003**, *83*, 1590.
(17) Liu, H.; Jiang, E. Y.; Bai, H. L.; Zheng, R. K.; Zhang, Wei, H. L.; Zhang, X. X. *Appl. Phys. Lett.* **2003**, *83*, 3531.
(18) Peng, D. L.; Asai, T.; Nozawa, N.; Hihara, T.; Sumiyama, K. *Appl. Phys. Lett.* **2002**, *81*, 4598.
(19) Venkatesan, M.; Nawka, S.; Pillai, S. C.; Coey, J. M. D. *J. Appl. Phys.* **2003**, *93*, 8023.
(20) Poddar, P.; Fried, T.; Markovich, G. *Phys. Rev. B* **2002**, *65*, 172405.
(21) Liu, K.; Zhao, L.; Klavins, P.; Osterloh, F. E.; Hiramatsu, H. *J. Appl. Phys.* **2003**, *93*, 7951.
(22) Wang, J.; Chen, Q.; Zeng, C.; Hou, B. *Adv. Mater.* **2004**, *16*, 137.
(23) Xue, D. S.; Zhang, L. Y.; Gao, C. X.; Xu, X. F.; Gui, A. B. *Chin. Phys. Lett.* **2004**, *21*, 733.
(24) Lian, S. Y.; Wang, E. B.; Kang, Z. H.; Bai, Y. P.; Gao, L.; Jiang, M.; Hu, C. W.; Xu, L. *Solid State Commun.* **2004**, *129*, 485.
(25) Han, S.; Li, C.; Liu, Z.; Lei, B.; Zhang, D.; Jin, W.; Liu, X.; Tang, T. *Nano Lett.* **2004**, *4*, 1241.
(26) Lind, D. M.; Berry, S. D.; Chern, G.; Mathias, H.; Testardi, L. R. *Phys. Rev. B* **1992**, *45*, 1838.
(27) Fujii, T.; de Groot, F. M. F.; Sawatzky, G. A.; Voogt, F. C.; Hibma, T.; Okada, K. *Phys. Rev. B* **1999**, *59*, 3195.
(28) Mott, N. F. *Metal−Insulator Transitions*, 2nd ed.; Taylor and Francis: London, 1990.

NL048758U